

Unveiling The Factors of Aesthetic Preferences with Explainable AI

Derya Soydaner^{1*} and Johan Wagemans¹

¹Department of Brain and Cognition, University of Leuven (KU
Leuven), Leuven, 3000, Belgium.

*Corresponding author(s). E-mail(s): derya.soydaner@kuleuven.be;
Contributing authors: johan.wagemans@kuleuven.be;

Abstract

The allure of aesthetic appeal in images captivates our senses, yet the underlying intricacies of aesthetic preferences remain elusive. In this study, we pioneer a novel perspective by utilizing machine learning models that focus on aesthetic attributes known to influence preferences. Through a data mining approach, our models process these attributes as inputs to predict the aesthetic scores of images. Moreover, to delve deeper and obtain interpretable explanations regarding the factors driving aesthetic preferences, we utilize the popular Explainable AI (XAI) technique known as SHapley Additive exPlanations (SHAP). Our methodology involves employing various machine learning models, including Random Forest, XGBoost, Support Vector Regression, and Multilayer Perceptron, to compare their performances in accurately predicting aesthetic scores, and consistently observing results in conjunction with SHAP. We conduct experiments on three image aesthetic benchmarks, providing insights into the roles of attributes and their interactions. Ultimately, our study aims to shed light on the complex nature of aesthetic preferences in images through machine learning and provides a deeper understanding of the attributes that influence aesthetic judgements.

Keywords: Machine learning, image aesthetics, regression, explainable AI

1 Introduction

Why do some images appeal to us while others evoke the opposite reaction? This question remains largely unanswered, as aesthetic preferences vary among individuals and depend on numerous factors. However, certain aesthetic attributes play a significant

role in shaping these preferences. Insights from diverse fields, including psychology and computer science, have contributed valuable knowledge on aesthetic preferences. In general, psychological studies in the field of empirical aesthetics have primarily focused on exploring the factors influencing aesthetic preferences [1]. In computer science, the emphasis has been on treating image aesthetic assessment as an artificial intelligence task, leading to models for classifying images based on aesthetic qualities or making aesthetic predictions [2]. The interdisciplinary field of computational aesthetics is a blend of these two disciplines, dedicated to developing computational methods for aesthetics research [3–5].

In this study, we adopt a machine learning approach to gain a deeper understanding of aesthetic preferences in images within the realm of computational aesthetics. Our unique perspective focuses on the influence of various attributes on aesthetic judgements. While many studies focus on image aesthetic assessment models that process image data as input and predict aesthetic-related scores as output (e.g., [6–12]), we take a novel approach by shifting our focus to aesthetic-related scores themselves. Instead of utilizing images as inputs, we develop regression models that take aesthetic attribute scores as inputs to predict the overall aesthetic scores of images. This alternative approach allows for a more detailed analysis of attribute information in aesthetic image datasets, providing valuable insights into the factors that contribute to aesthetic preferences. To enhance the interpretability of these regression models, we employ the SHapley Additive exPlanations (SHAP) method [13], an Explainable AI (XAI) technique specifically designed to provide insights into the contributions of individual attributes to the model’s output. Our investigation goes beyond the overall effects of attributes and explores their interactions as well.

While SHAP effectively highlights the importance of each attribute on the model’s predictions, it does not assess prediction quality itself. To comprehensively evaluate our approach, we employ a diverse set of machine learning models. Specifically, we utilize two ensemble machine learning models, namely Random Forest and eXtreme Gradient Boosting (XGBoost), along with a kernel-based regression model known as Support Vector Regression. Additionally, we incorporate a neural network approach, specifically the Multilayer Perceptron, which is particularly well-suited for regression problems. By employing multiple models and consistently observing results in conjunction with SHAP, we establish a reliable interpretation of the effects of image aesthetic attributes. Furthermore, we evaluate our approach on three image aesthetic benchmarks. Since only three benchmarks in the literature include aesthetic attribute information, we utilize them to explore attributes and identify similarities across datasets.

We summarize the key contributions of this work as follows.

- We introduce a novel perspective by utilizing machine learning models for regression to gain insights into aesthetic preferences in images.
- To the best of our knowledge, we pioneer the utilization of attribute information in image aesthetic benchmarks through a data mining approach, providing a deeper analysis of the role of attributes in aesthetic judgements.
- We provide the first detailed comparative analysis of various machine learning models within the computational aesthetics field, exploring their performance in predicting aesthetic scores.

- We present the first application of the SHAP method in understanding image aesthetics, enhancing the interpretability of machine learning models and unveiling the contributions of individual attributes to aesthetic predictions.

2 Methodology

In this study, our objective is to gain insights into image aesthetic preferences through a data mining approach. To achieve this, we leverage the SHAP method, a popular XAI technique, to provide explanations for our models. Our methodology comprises two main steps: first, training a machine learning model that takes aesthetic attributes as inputs to predict the overall aesthetic scores of images, and subsequently employing the SHAP method to explain the importance of these inputs in predictions. Figure 1 illustrates the general overview of our approach.

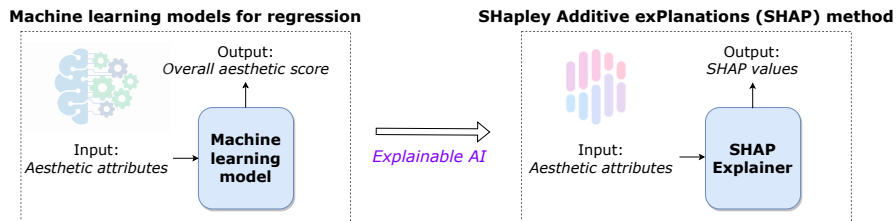


Fig. 1 Overview of our approach: Training a machine learning model using various aesthetic attribute scores to predict overall aesthetic score, and then employing a SHAP explainer based on the trained machine learning model to compute SHAP values for the same attributes.

We employ a diverse range of machine learning models, comparing their performances, and then examining the SHAP results of the model that achieves the most accurate predictions. This section provides a detailed explanation of the models we employ in this study, along with an in-depth description of how we leverage the SHAP method to gain insights into the attributes driving aesthetic preferences.

We begin by implementing ensemble methods that utilize decision trees, specifically Random Forest and XGBoost. Ensemble learning is a widely used technique in machine learning that combines multiple individual models to create a more accurate predictive model. The core idea behind ensemble learning is to combine predictions from diverse models, leveraging the strengths of each model while mitigating their weaknesses. The individual models within the ensemble can be of the same type, such as multiple decision trees, or they can be different types, such as a combination of decision trees, support vector machines, and neural networks.

Continuing with our methodology, we incorporate a kernel-based approach, specifically Support Vector Regression [14], which leverages the powerful mathematical foundations of support vector machines [15] to capture intricate relationships within the data. Additionally, we develop a Multilayer Perceptron, a neural network architecture known for its suitability in regression tasks. By employing these diverse machine learning models, we provide a comprehensive analysis of them to gain insights into their predictive capabilities.

Through this analysis, our objective is to identify the model that demonstrates the highest performance in predicting image aesthetics. Once the best performing model is determined, we proceed with the utilization of the SHAP method to interpret the importance of attributes in predicting the overall aesthetic score. By applying the SHAP method, we aim to gain insights into the factors influencing image aesthetics and enhance the interpretability of the regression models.

2.1 Machine learning models for regression

Our focus is predicting aesthetic scores of images, i.e., a regression task. Therefore, the machine learning models discussed in this section are primarily utilized for regression purposes. As a reminder, the main distinction between regression and classification tasks lies in the nature of the output: regression tasks aim at predicting continuous values, while classification tasks are about determining the discrete class labels an input belongs to. It is important to note that machine learning models detailed in this section can also be applied to classification tasks. However, in our research, we specifically implement them within the context of regression.

2.1.1 Random Forest

Random Forest, also known as Random Decision Forest, was initially introduced by Ho (1995) [16] as an ensemble learning method. It constructs multiple decision trees in randomly selected subspaces of the feature space. Decision trees are powerful models for classification and regression tasks; for more detailed information, see [17, 18].

The concept of Random Forest was further developed by Breiman (2001) [19], building upon the principles of *bagging*. In bagging, the same training algorithm is applied to each predictor, but they are trained on different random subsets of the training set. When sampling is performed *with* replacement, this method is referred to as bagging [20] in machine learning, or *bootstrapping* in statistics. Conversely, when sampling is performed *without* replacement, it is known as *pasting*. Random Forest is an ensemble of decision trees that are typically trained using the bagging method, and occasionally with pasting as an alternative approach [18].

Random Forest constructs multiple decision trees, each trained on different random subsets of the training data. This results in a diverse set of predictors working collectively to make predictions. Once all predictors are trained, the ensemble can make a prediction for a new instance by computing mean or average prediction across the individual trees, particularly for regression tasks. Random Forest incorporates additional randomness during the tree-growing process. Instead of searching for the optimal feature when splitting a node, it selects the best feature among a random subset of features [18]. This strategy often leads to a more robust and improved model.

2.1.2 XGBoost

eXtreme Gradient Boosting, commonly known as XGBoost, is another ensemble learning method that combines the predictions of multiple models to enhance prediction accuracy [21]. It is built upon the principles of *boosting* [22], an ensemble technique widely used in machine learning. Boosting methods train predictors sequentially, with

each subsequent model aiming to correct the errors of its predecessor. One popular boosting algorithm is *Gradient Boosting*, which integrates predictors incrementally into the ensemble. Each new predictor aims to reduce the *residual errors* generated by the preceding predictor [18]. More specifically, each model tries to predict the residuals calculated by its predecessor, using a gradient descent algorithm to minimize the loss.

XGBoost is a scalable machine learning framework specifically designed for *tree* boosting [21]. This algorithm constructs decision trees sequentially, and iteratively adds them to the ensemble while optimizing a loss function. Each subsequent tree is built to correct the errors made by the preceding trees. XGBoost learns through gradient boosting, which updates the model's parameters using gradients to minimize the loss function. Therefore, XGBoost can be regarded as an implementation of gradient tree boosting [23], effectively combining the strengths of decision trees and gradient-based optimization techniques.

XGBoost is known for its high predictive accuracy, scalability, and flexibility. It places significant emphasis on the use of weights, which are assigned to all independent variables, and fed into the decision tree during prediction process. Notably, XGBoost employs a strategy where the weights of variables that were incorrectly predicted by the tree are increased, and these adjusted variables are then passed on to the subsequent decision tree. This ensemble of individual predictors results in a strong and precise model. Additionally, it incorporates both L^1 and L^2 regularization techniques, providing effective control and penalization of the model. To elaborate, regularization is a technique used to prevent *overfitting*, which occurs when the model performs well on training data, yet poorly on test data. Goodfellow *et al.* (2016) [24] provides a comprehensive exploration of regularization techniques.

2.1.3 Support Vector Regression

Support Vector Regression (SVR) [14] is a widely used machine learning method for regression tasks. It is rooted in the principles of Support Vector Machines (SVMs) [15], with the objective of finding a hyperplane that best fits the training data while minimizing the error. This hyperplane is defined by a set of *support vectors*, which are data points located closest to the boundary of the hyperplane. The distance between the support vectors and the hyperplane is known as the *margin*. In SVR, the aim is to position as many instances as possible on the hyperplane while controlling margin violations, which occur when instances fall outside the margin. The width of the hyperplane is controlled by the parameter ϵ [18].

This approach brings the advantage of effectively capturing nonlinear dependencies, leading to improved performance [25]. To handle non-linear regression problems efficiently, SVR employs a key concept known as the *kernel trick*. The kernel trick becomes necessary when the input data cannot be linearly separated in its original feature space. It allows SVR to implicitly map the input data into a higher-dimensional feature space, where it becomes linearly separable. This mapping is achieved using a kernel function, which computes the dot product between pairs of data points in the higher-dimensional space without explicitly calculating the transformed feature vectors. One commonly used kernel function in SVR is the Radial Basis Function (RBF) kernel, defined as:

$$\begin{aligned}
K(x, x') &= \exp\left(-\frac{\|x - x'\|^2}{2\sigma^2}\right) \\
&= \exp(-\gamma\|x - x'\|^2)
\end{aligned}
\tag{1}$$

where, x and x' represent input data, $\|x - x'\|^2$ denotes the squared Euclidean distance between them, and γ is the kernel coefficient that controls the smoothness of the kernel function. Eq. 1 measures the similarity or dissimilarity between two data points based on their distance in the input feature space. It assigns higher similarity values to data points that are closer together and lower similarity values to those that are farther apart. By utilizing kernel functions, SVR can effectively find a linear hyperplane in this transformed space, enabling accurate regression predictions even when the original feature space lacks a linear relationship.

2.1.4 Multilayer Perceptron

Our final machine learning model for predicting aesthetic scores is a neural network, specifically a Multilayer Perceptron (MLP), which is well-suited for regression tasks. It is a feedforward neural network with one or more hidden layers between the input and output layers, enabling it to extract meaningful features from the data.

The training process of an MLP involves two main steps: the forward pass and the backward pass. During the forward pass, the input is fed into the input layer, and each hidden layer computes a weighted sum of its inputs, followed by the application of an activation function. The activations then propagate forward through the network. An error is then computed using a loss function that compares predictions with ground-truth labels. In the backward pass, known as backpropagation [26], the gradients of errors with respect to the network’s weights are computed. These gradients are then used in the learning process, where an algorithm, usually called as an *optimizer*, updates the weights to minimize the error [24]. For a more detailed explanation of MLP and its training process, see [27].

Neural networks, including the MLP, are powerful models in machine learning, particularly within the subfield of deep learning. They have gained immense popularity due to their ability to leverage multiple hidden layers and learn intricate representations from raw data. Deep learning has revolutionized various domains and led to significant advancements in artificial intelligence, achieving breakthroughs in various fields such as natural language processing [28], and computer vision [29, 30].

2.2 Explainable AI

With the widespread adoption of AI techniques, there has been an increasing demand for explanations and transparency. Machine learning models have often been criticized as ‘black box’ systems. This critique becomes particularly concerning when employing these models to gain insights about human intelligence and task performance. Addressing this need, the field of explainable AI (XAI) has gained significant attention [31–34]. XAI can be used as a useful tool to augment the psychological insight gained from machine learning models, thereby enhancing the utility of AI as a valuable source in psychology.

Several XAI techniques have been proposed such as Local Interpretable Model-agnostic Explanations (LIME) [35] and Deep Learning Important FeaTures (DeepLIFT) [36]. One prominent technique that has achieved widespread recognition is SHapley Additive exPlanations (SHAP) [13]. SHAP values, the key component of this technique, prove to be more consistent with human intuition than other techniques that fail to meet three desirable properties for a single unique solution: local accuracy, missingness, and consistency [13]. SHAP is a game-theoretic approach designed to explain the outputs of machine learning models, providing insights into the contribution of each feature to the model’s predictions. By assigning SHAP values to features, which represent their relative importance compared to a baseline reference, this approach enables a comprehensive understanding of the factors that influence the model’s output. Consequently, SHAP enhances the interpretability and transparency of AI systems.

The Shapley value, originally introduced by Shapley [37], is a concept in Game Theory that assigns payouts to players based on their individual contributions to the total payout within a cooperative coalition. The concept of Shapley values has been extensively studied in Game Theory literature [38] and has emerged as a principled framework for obtaining feature attributions as explanations. In the context of XAI, the features of the model are treated as the players, while the prediction itself represents the ‘game’. By employing the SHAP method, we aim to determine the extent to which each feature, or ‘player’ in the context of the coalition, contributes to the overall prediction.

The SHAP explanation method leverages the concept of Shapley values derived from coalitional game theory to quantify the contributions of individual features in a machine learning model. Shapley values provide a measure of the influence each feature has on the model’s predictions, offering insights into how the ‘payout’ (i.e., the prediction) should be fairly distributed among the features [39]. Since the exact computation of SHAP values is challenging, Lundberg and Lee (2017) [13] introduced model-type-specific approximation methods. Among these, *KernelSHAP* is designed for kernel-based models like Support Vector Regression, while *TreeSHAP* is a highly efficient approach tailored for tree-based models such as Random Forest. These approximation methods enable the computation of SHAP values, facilitating the interpretation and explanation of predictions in various types of models.

Despite the usefulness and widespread adoption of the SHAP method, one major challenge in utilizing Shapley values for model explanation is the significant computation time [40], which grows exponentially with the number of features involved [39]. Fortunately, SHAP performs efficiently for tree-based machine learning models like XGBoost and Random Forest, as well as for the relatively simpler MLP used in our study. However, it becomes notably slow for Support Vector Regression. Managing the computational cost of SHAP becomes crucial, particularly when dealing with models involving a large number of features, and we will discuss potential mitigations and their implications in the subsequent sections.

The SHAP method offers versatility in visualizing and interpreting its results, making it applicable across various domains. While SHAP has been utilized in different areas, such as explaining image models [41], our study pioneers its application in

understanding aesthetic preferences for images. By employing SHAP in this novel context, we aim to shed light on the underlying factors that contribute to image aesthetics and provide insights into the subjective nature of aesthetic judgments.

3 Datasets

In this study, we use three publicly available datasets specifically designed for image aesthetic assessment. These datasets include diverse attributes that are known to influence aesthetic preferences. Notably, each dataset not only provides overall aesthetic scores for images but also includes attribute scores, making them ideal for regression modeling. We provide a detailed description of each dataset, highlighting their unique characteristics and relevance to our research objectives. By leveraging these datasets, we aim to gain comprehensive insights into the factors influencing image aesthetics.

AADB. We begin with the Aesthetics with Attributes Database (AADB) [42], which serves as a widely recognized image aesthetic benchmark. This dataset comprises 10,000 RGB images sourced from the Flickr website, each with a size of 256×256 pixels. Each image in the AADB dataset is accompanied by an overall aesthetic score provided by five different raters. Kong *et al.* (2016) [42] reported the average aesthetic scores provided by these raters for each image, which serve as the ground-truth scores. These scores range from 1 to 5, with 5 representing the most aesthetically pleasing score.

Moreover, the AADB dataset includes eleven attributes that professional photographers have identified as influential in aesthetic judgements. These attributes are balancing element, interesting content, color harmony, shallow depth of field, good lighting, motion blur, object emphasis, rule of thirds, vivid color, repetition, and symmetry. Notably, each image in the AADB dataset is associated with scores for each attribute. Raters indicated whether each attribute has a positive, negative, or null (zero) effect on the aesthetics of an image, except for repetition and symmetry, where only the presence or absence of the attribute is rated. The raters were not permitted to assign negative scores for repetition and symmetry.

The scores provided in the AADB dataset are presented in normalized form. The average scores are normalized within the range of $[0, 1]$, while all attributes, excluding repetition and symmetry, are normalized within the range of $[-1, 1]$. Repetition and symmetry scores, on the other hand, are normalized within the range of $[0, 1]$. Figure 2 illustrates two sample images from the training set of the AADB dataset, showcasing examples of both low and high aesthetics. The figure includes the corresponding overall aesthetic scores as well as attribute scores.

The AADB dataset has been officially partitioned into three subsets, as described by Kong *et al.* (2016) [42]. Specifically, the dataset is divided into 500 images for validation, 1000 images for testing, and the remaining images for training. In our experiments, we use this official partition to train and evaluate our machine learning models.

EVA. The Explainable Visual Aesthetics (EVA) dataset [43] is a comprehensive collection of 4070 images, each of which has been rated by a minimum of 30 participants. Within the EVA dataset, each image receives between 30 to 40 votes. These ratings

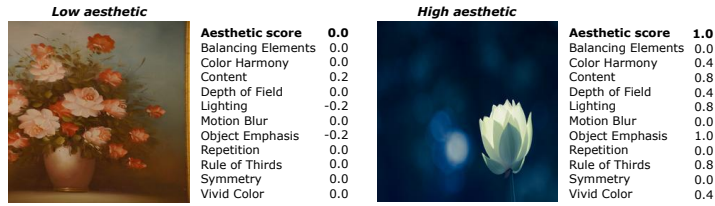


Fig. 2 Example images from the training set of the AADB dataset. Each image has an overall aesthetic score and scores for 11 attributes. (*Left*) Low aesthetic: An image rated with the lowest overall aesthetic score. (*Right*) High aesthetic: An image rated with the highest overall aesthetic score. It is important to note that the AADB dataset includes multiple images with overall aesthetic scores of 0.0 and 1.0. We randomly selected two examples for illustration.

are assigned on an 11-point discrete scale, with the extremes of the scale labeled as ‘least beautiful’ (corresponding to 0) and ‘most beautiful’ (corresponding to 10). Alongside the aesthetic ratings, the EVA dataset includes four attributes: light and color, composition and depth, quality, and semantics of the image. Participants provided ratings for each attribute on a four-level Likert scale, ranging from ‘very bad’ to ‘bad,’ ‘good,’ and ‘very good.’ Figure 3 presents two sample images from the EVA dataset, illustrating examples of both low and high aesthetic images.

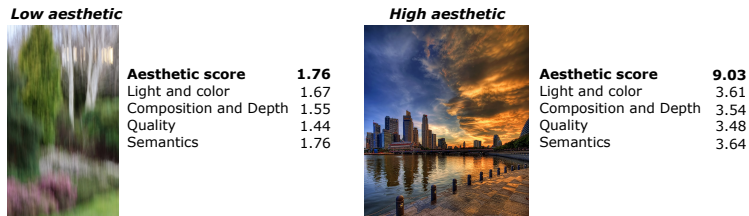


Fig. 3 Example images from the training set of the EVA dataset. Each image has an overall aesthetic score and scores for 4 attributes. (*Left*) Low aesthetic: The image rated with the lowest overall aesthetic score. (*Right*) High aesthetic: The image rated with the highest overall aesthetic score.

In contrast to the AADB dataset, Kang *et al.* (2020) [43] provided the complete set of ratings from the participants for each image in the EVA dataset. In order to facilitate our analysis, we calculated the average scores based on these ratings. Unlike the AADB dataset, which offers predefined train-validation-test splits, the EVA dataset does not have an official partition. This is because Kang *et al.* (2020) did not employ any specific prediction model. As a result, we align our approach with previous studies that focus on image aesthetic assessment using the EVA dataset. In the literature, different training and testing splits have been applied for the EVA dataset [44, 45]. For our experiments, we follow the three studies [9, 11, 46], which use 3,500 images for training and 570 for testing.

PARA. The final dataset utilized in this study is the Personalized image Aesthetics database with Rich Attributes (PARA) [47], which consists of 31,220 images collected

from CC search¹. To ensure a diverse range of content, the authors employed a pre-trained scene classification model to predict scene labels for the images. Subsequently, approximately 28,000 images were selectively sampled based on these predicted labels.

To further refine the aesthetics score distribution, the PARA dataset was augmented with around 3,000 additional images. These additional images were selected to provide clear aesthetics ground truth and were sourced from Unsplash², as well as image quality assessment databases such as SPAQ [48] and KonIQ-10K [49]. The aim of this augmentation process was to achieve a balanced representation of aesthetics scores across the dataset, ensuring a comprehensive and diverse collection of images suitable for analysis.

Each image in the PARA dataset has been annotated by 25 subjects on average, with a total of 438 subjects contributing to the annotations. Each image is annotated with 4 human-oriented subjective attributes (emotion, difficulty of judgement, content preference, and willingness to share) and 9 image-oriented objective attributes (aesthetics, quality, composition, color, depth of field, content, light, object emphasis, and scene categories). In our study, we aim to predict the aesthetics scores using the image-oriented objective attributes (excluding the scene categories) as inputs for our regression models. We do not include the human-oriented subjective attributes and scene categories as the inputs, since they are considered irrelevant for our specific research objective. By utilizing these seven inputs, our machine learning models predict the aesthetic scores of the images. A summary of the attributes used as inputs for the machine learning models in this study, including those from the PARA dataset and other datasets, is provided in Table 1.

Table 1 Image aesthetic benchmarks and their corresponding attributes used in this study.

Datasets	Attributes
AADB [42]	Balancing elements, color harmony, content, depth of field, light, motion blur, object emphasis, repetition, rule of thirds, symmetry, vivid color
EVA [43]	Light and color, composition and depth, quality, semantics
PARA [47]	Quality, composition, color, depth of field, light, content, object emphasis

The image-oriented attributes in the PARA dataset are mostly discretely annotated on a scale from 1 to 5. Specially, the object emphasis attribute is represented by a binary label, indicating the presence or absence of a salient object within the image. The aesthetics score is assigned as a discrete class label, ranging from 1 to 5, reflecting the comprehensive judgement of visual aesthetics. To address ambiguity, Yang *et al.* (2022) [47] introduced an additional option between each integer value. A higher aesthetics score indicates better visual aesthetics perception. The quality score represents the overall judgement of image quality, also ranging from 1 to 5. A higher quality score denotes a better perceptual quality. It is worth mentioning that images with low perceptual quality in the PARA dataset exhibit various degradations, such

¹<https://search.creativecommons.org/>

²Unsplash, <https://unsplash.com/>

as motion blur, JPEG compression, and others. Figure 4 presents two sample images from the PARA dataset, illustrating examples of both low and high aesthetic images.

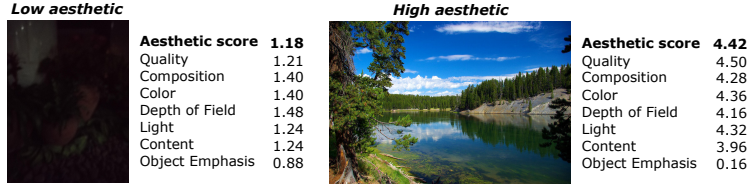


Fig. 4 Example images from the training set of the PARA dataset. Each image has an overall aesthetic score and scores for 7 attributes. (*Left*) Low aesthetic: The image rated with the lowest overall aesthetic score. (*Right*) High aesthetic: The image rated with the highest overall aesthetic score.

4 Implementation details

We conducted a systematic experimentation process, comparing the performance of four regression models: Random Forest, XGBoost, SVR, and MLP. Our goal is to find the model that achieves the highest performance, which we subsequently analyze in detail using the SHAP method. Each regression model is trained on three separate datasets, as outlined in Section 3. We employ appropriate hyperparameter configurations for each model, which are provided below. These specific hyperparameter settings are chosen based on empirical evidence and commonly accepted practices in the field of machine learning. Subsequently, we evaluate each trained model based on the performance metrics described in Section 5.

4.1 Model Hyperparameter Details for Random Forest

We outline the main hyperparameters and their corresponding values for the Random Forest model in our experiments. The first hyperparameter, *number of estimators*, determines the number of decision trees within the random forest. In our implementation, we set this parameter to 150, indicating the construction of 150 decision trees. Bootstrap samples, known as bagging in machine learning literature, are utilized during the tree-building process (see Section 2.1.1). The *criterion* parameter is a crucial factor in determining the split quality at each node within the decision trees. In our study, we utilize the mean squared error as the criterion to guide the splitting process.

The *maximum depth* parameter controls the depth of the decision trees. By default, when set to ‘None’, the trees continue growing until all leaves are pure or until the number of samples within a leaf falls below the *minimum samples split* threshold. This threshold determines the minimum number of samples required to initiate a split at an internal node. With a default value of 2, a node will only be split if it contains at least two samples. In our experiments, we do not explicitly set a maximum depth, allowing the trees to grow until these conditions are met. Similarly, the *minimum samples leaf* parameter sets the minimum number of samples required for a node to be considered a leaf. In our implementation, we utilize a default value of 1, indicating that even the

smallest node is eligible to be classified as a leaf. Additionally, the *maximum features* parameter controls the number of features considered when searching for the best split. In our experiments, we set the default value to ‘auto’, which selects the square root of the total number of features for consideration during the split selection process.

4.2 Model Hyperparameter Details for XGBoost

We present the specific hyperparameter details for XGBoost used in our experiments. The *number of estimators*, corresponding to the number of boosting rounds or decision trees constructed, is set to 150 in our implementation. Each decision tree within the ensemble has a maximum depth of 3, limiting the complexity and depth of the individual trees. The *learning rate* is applied to each boosting iteration is set to 0.1. This parameter controls the contribution of each tree within the ensemble, striking a balance between the learning speed and the model’s ability to generalize.

In our experiments, we use a *subsample* value of 1, indicating that the entire training dataset is used for constructing each tree within the ensemble. To introduce regularization and prevent overfitting, we incorporate the L1 and L2 regularization terms on the weights, with values of 0 and 1, respectively. The mean squared error is employed as the loss function to be minimized during training, while the root mean squared error served as the evaluation metric for validation during the training process.

4.3 Model Hyperparameter Details for Support vector regression

We provide an overview of the specific hyperparameters and their settings for SVR employed in our experiments. The choice of kernel function is crucial for mapping the input data to a higher-dimensional feature space. We utilized the radial basis function (RBF) kernel, which is a popular choice for SVR. The regularization parameter, denoted as C , balances the trade-off between maximizing the margin and minimizing the training error. A smaller C value results in a wider margin but may lead to more margin violations [18]. In our experiments, we set C to 1.0, striking a balance between margin width and training error. The ϵ parameter defines the margin of tolerance within which no penalty is given to errors in the epsilon-insensitive loss function. We set ϵ to 0.01, determining the acceptable range where errors are not penalized.

The kernel coefficient (γ) determines the influence of each training example, with higher values of γ result in closer training examples having a stronger influence. We set γ to ‘scale’, which automatically calculates an appropriate value based on the inverse of the feature scale. The *tolerance* for the stopping criterion, indicating the desired precision for convergence, is set to 1e-3. Lastly, the maximum number of iterations to perform is set to -1, indicating no explicit limit on the number of iterations. The algorithm continues until the convergence criteria are met.

4.4 Model Hyperparameter Details for Multilayer perceptron

In this study, our MLP architecture consists of one hidden layer with 32 hidden units. We determined this architecture through an iterative process, experimenting with different depths and numbers of hidden units. We found that using one hidden layer

with 32 units is sufficient for achieving good performance while avoiding overfitting. Since we predict the aesthetic scores, which is a single numerical value, the output layer includes 1 unit. The hidden layer employs the Rectified Linear Unit (ReLU) [50] activation function, while the output layer applies a linear function. ReLU activation outputs the input itself if it is positive; otherwise, it outputs zero. Linear activation in the output layer is often used in regression tasks where the goal is to predict a continuous value, and there is no need to map the output to a specific range or set of classes. We initialize the layer weights using the Glorot normal initializer, also known as Xavier normal initializer [51]. We train our MLP architecture for 40 epochs using Adam algorithm [52] to minimize mean squared error. The minibatch size is set to 64. The Adam algorithm is an adaptive gradient method that individually adapts the learning rates of model parameters [52]. During training, the Adam algorithm calculates the estimates of the first and second moments of the gradients and then utilizes decay constants to update them. These decay constants are additional hyperparameters along with the learning rate. More detailed information about the adaptive gradient methods in deep learning can be found in [53]. In our study, the initial learning rate is 0.001, and decay constants are 0.9 and 0.999, respectively.

5 Experimental results

In this section, we present the experimental results, following the methodology outlined in Fig. 1. Initially, we develop individual machine learning models for each dataset to assess their performances in predicting overall aesthetic scores. For this evaluation, we report standard evaluation metrics, including the coefficient of determination (R-squared), mean absolute error (MAE), mean squared error (MSE), and root mean squared error (RMSE). Additionally, we report Spearman’s rank correlations (ρ), which is significant at $p < 0.01$ in our analysis. These metrics serve as reliable indicators of the accuracy and goodness of fit of our models.

After evaluating the models, we identify the one that demonstrates the highest predictive capability among them. Subsequently, we conduct a detailed examination of the results from this model using the SHAP method. By utilizing this XAI technique, we aim to gain a better understanding of the importance of individual attributes in predicting overall aesthetics scores.

5.1 Analysis Results on the AADB Dataset

We begin our analysis with the AADB dataset [42], which is the oldest among the three image aesthetic assessment datasets described in Section 3. For our regression task, we train four different machine learning models described in Section 2.1. Using the attribute scores as inputs (Table 1), these models predict the overall aesthetic scores of the images. Performance comparison of these models is based on various metrics, including the R^2 coefficient, MAE, MSE, RMSE, and ρ between the predicted overall aesthetic scores and the ground-truth scores, presented in Table 2. In general, all machine learning models demonstrate good performance on the AADB dataset. However, the MLP and SVR models perform slightly better than the others, with SVR demonstrating a slightly superior performance compared to MLP.

Table 2 Performance of four machine learning models on the AADB dataset. We calculate all metrics on the test data to evaluate generalization ability.

Model	R^2	MAE	MSE	RMSE	ρ
Random forest	0.8320	0.0704	0.0077	0.0877	0.924
Multilayer perceptron	0.8645	0.0620	0.0062	0.0787	0.939
XGBoost	0.8492	0.0663	0.0069	0.0831	0.935
Support vector regression	0.8684	0.0620	0.0060	0.0776	0.939

Next, we apply the SHAP method to analyze the results of the SVR model on the AADB dataset. We calculate SHAP values for the test data, with each SHAP value representing the contribution of an individual feature to the model’s output. We present a summary of the SHAP values in Figure 5. This SHAP summary plot provides a visual illustration of the impact of each feature on the predictions made by the SVR model. The features are listed on the y-axis of the plot, ranked by their importance, with the most influential feature at the top and the least influential at the bottom.

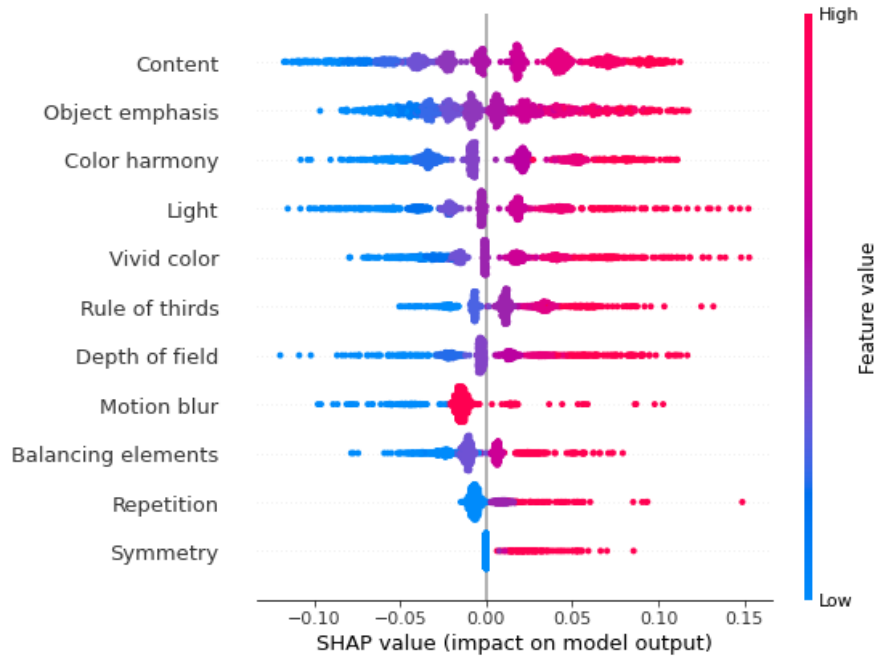


Fig. 5 Shap summary plot for the AADB dataset based on the SVR model.

According to the results, the attribute ‘content’ emerges as the most influential feature in predicting the overall aesthetic scores. It is followed by ‘object emphasis’ and ‘color harmony’, both of which also make significant contributions to the predictions. It is worth noting that these top three inputs include two high-level attributes and one

mid-level attribute. On the other hand, ‘repetition’ and ‘symmetry’ are observed to have minimal impact on predicting the overall aesthetic scores, as evidenced by their placement at the bottom of the plot. It is important to consider that in the AADB dataset, repetition and symmetry attributes are predominantly rated as neutral, which might explain their lower impact. Additionally, despite the attribute ‘motion blur’ being mostly rated as neutral, it ranks fourth from the bottom in terms of importance. Further insights into the distribution of attributes in the AADB dataset can be found in Appendix A.

The SHAP values in Figure 5 quantify the contribution of each attribute to individual predictions. By examining the x-axis, we can assess the relative importance of features based on their SHAP values. Features with larger absolute SHAP values have a more substantial impact on the model’s predictions, while those with smaller absolute SHAP values have a relatively minor impact. Each attribute is represented by a horizontal bar on the graph. The length of the bar corresponds to the magnitude of the SHAP values. The color of the bar represents the direction of the feature’s impact on the output: blue indicates a lower feature value, while red indicates a higher feature value. The color intensity reflects the magnitude of the feature value.

Due to the significant computation time required to compute SHAP values for the SVR model, we followed the recommendation in the official SHAP documentation³ and applied k-means clustering to the training set. We summarized the training set with three clusters using k-means, with each cluster weighted by the number of points it represents. We also adopt the same k-means approach to examine the SHAP summary plot for the MLP model. For the other models (Random Forest and XGBoost), we directly examine the SHAP summary plots using the entire dataset without applying k-means. Remarkably, all these machine learning models consistently yielded similar results in terms of attribute rankings. In every case, the ‘content’ attribute emerged as the most influential in predicting the overall aesthetic score across all models. On the other hand, the ‘symmetry’ attribute consistently appeared at the bottom of the plot, indicating its minimal impact on the model’s predictions. For the other three models, except SVR, the ‘color harmony’ attribute ranked second, followed by the ‘object emphasis’ attribute. We can interpret this result as these two attributes having a similar level of importance in influencing the model’s predictions. The ranking of the other attributes varied slightly across the models, but there were no striking changes in the overall results. For SHAP summary plots of the other machine learning models (Random Forest, XGBoost, and MLP), please refer to Appendix B.

SHAP values not only provide valuable insights into the individual contributions of features but also enable the examination of interactions between features. Interaction plots illustrate how two features jointly influence the model’s prediction. Similar to the SHAP summary plot, in an interaction plot, a more intense red color indicates higher positive SHAP values, while a more intense blue color indicates lower negative SHAP values. When the interaction plot shows more red, it suggests that both features together positively contribute to the model’s prediction. High values of both features together tend to increase the model’s output, and the interaction between these features strengthens their combined effect in a positive direction. Conversely, when the

³<https://shap-lrjball.readthedocs.io/en/latest/examples.html>

interaction plot exhibits more blue, it indicates that both features together contribute negatively to the model’s prediction. Low values of both features together tend to decrease the model’s output, and the interaction between these features strengthens their combined effect in a negative direction. The intensity of the colors reflects the strength of the interaction between the two features, indicating the magnitude of their combined impact on the model’s prediction. Overall, by examining the interaction plots and observing the color patterns, we can gain insights into how two features interact and jointly influence the model’s predictions. This helps to identify important feature combinations and understand how the model makes decisions based on their joint values.

In the AADB dataset, which comprises a total of 11 attributes, there are many potential interactions between these attributes. In Figure 6, we present some striking examples of the interactions observed in the SHAP values between aesthetic attributes. For example, we observe more positive interactions between balancing elements and content, as well as color harmony and content, and depth of field and object emphasis. These interactions suggest that when both of these attributes exhibit high values together, they tend to have a positive influence on the model’s prediction, and their combined effect reinforces the model’s output.

On the other hand, we see extremely positive interactions between attributes like balancing elements and motion blur, color harmony and motion blur, content and motion blur, depth of field and motion blur, and light and motion blur. Motion blur appears to have a significant interaction with several other attributes, implying its importance when combined with these features in determining the overall aesthetic score. We present the rest of the interaction plots in Appendix C.

5.2 Analysis Results on the EVA Dataset

We continue our analysis with the EVA dataset. This time, we utilize four attribute scores as inputs for our machine learning models to predict the overall aesthetic scores of images. The results are presented in Table 3. While Random Forest performs slightly behind the other models, the remaining three models exhibit similar performance. Once again, SVR demonstrates slightly better performance, which leads us to apply the SHAP method to the SVR model to gain deeper insights into the importance of individual attributes in predicting overall aesthetic scores.

Table 3 Performance of four machine learning models on the EVA dataset. We calculate all metrics on the test data to evaluate the generalization ability.

Model	R^2	MAE	MSE	RMSE	ρ
Random forest	0.9285	0.2230	0.0779	0.2792	0.963
Multilayer perceptron	0.9313	0.2113	0.0749	0.2737	0.966
XGBoost	0.9321	0.2133	0.0740	0.2720	0.965
Support vector regression	0.9342	0.2100	0.0718	0.2679	0.965

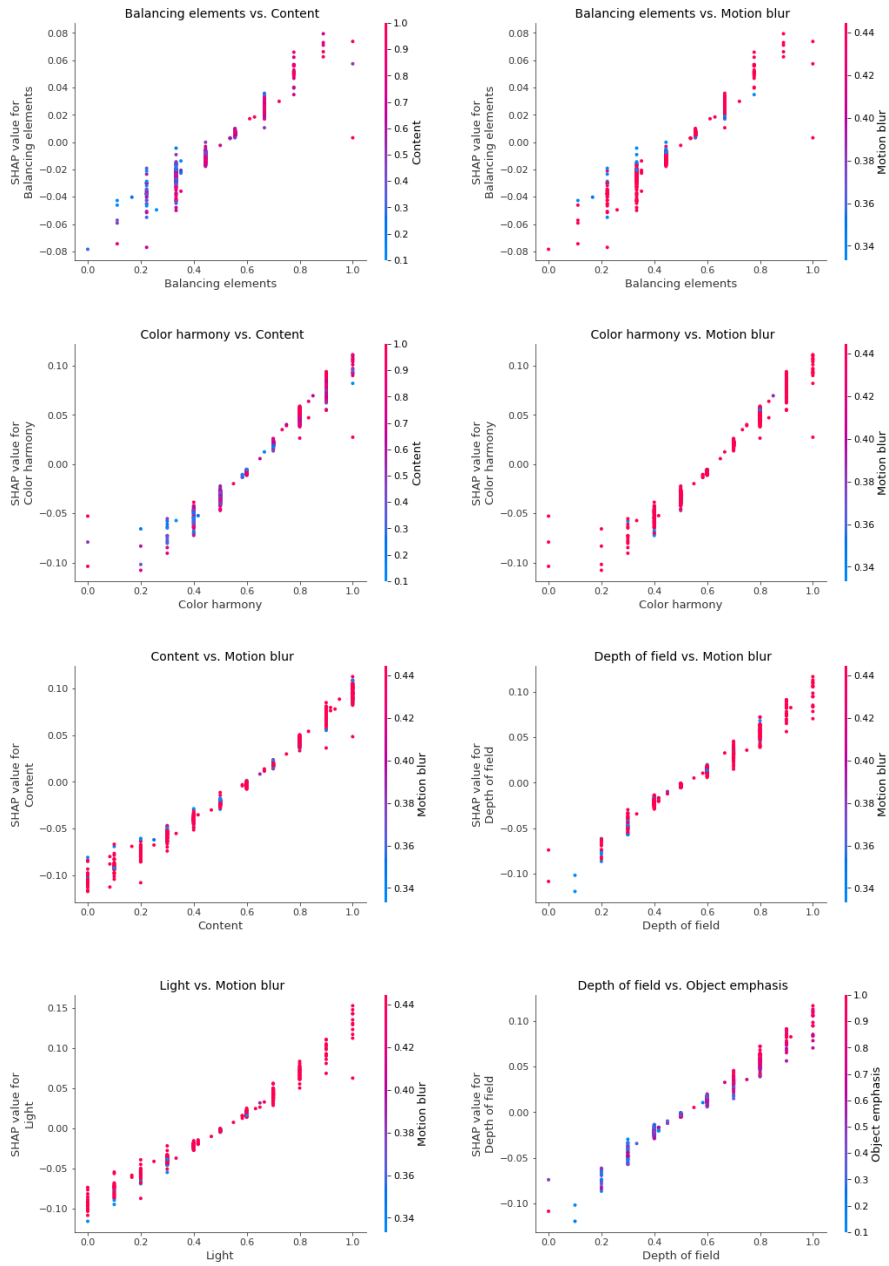


Fig. 6 Selected attribute interaction plots for the AADB dataset based on the SVR model.

We present the SHAP summary plot for the EVA dataset in Figure 7. According to the results, the attribute ‘semantics’ emerges as the most important feature in predicting the overall aesthetic scores. It is followed by ‘light and color’, ‘composition

and depth’, and ‘quality’, respectively. Interestingly, we observe some parallels between the results obtained from the EVA and AADB datasets. In the AADB dataset, color harmony and light attributes are ranked third and fourth in importance, while in the EVA dataset, the second most important attribute in predicting the overall aesthetic score is ‘light and color’. It is worth noting that each image in the EVA dataset has more ratings compared to the AADB dataset.

In the SHAP summary plots based on our Random Forest, XGBoost, and MLP models, we consistently find ‘semantics’ ranked first and ‘quality’ ranked last. However, ‘light and color’ consistently appears in the second place, while ‘composition and depth’ consistently appears in the third place. For SHAP summary plots of these machine learning models, please refer to Appendix D.

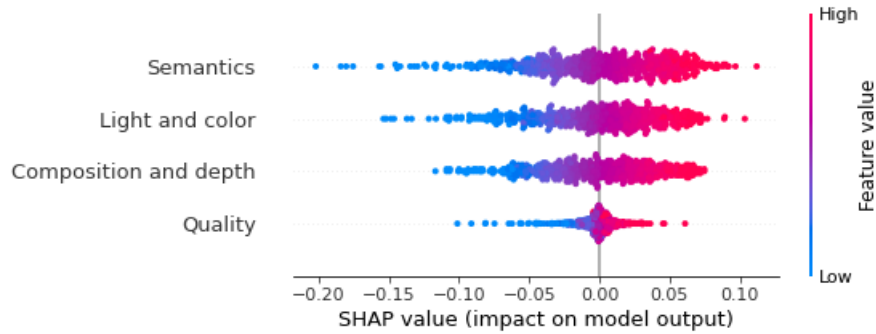


Fig. 7 Shap summary plot for the EVA dataset based on SVR model.

The interaction plots for attributes in the EVA dataset are presented in Figure 8. Since the EVA dataset has only four attributes as inputs, we have a smaller set of plots to examine compared to the AADB dataset discussed in the previous section. In all the interaction plots for the EVA dataset, we observe that high values of each feature combination tend to increase the model’s output. Specifically, when the ‘light and color’ score is around 0.4, its interaction with ‘composition and depth’, ‘quality’, and ‘semantics’ strengthens their combined effect in a positive direction, respectively. Similarly, when the ‘composition and depth’ score is around 0.5, it exhibits interactions with ‘quality’ and ‘semantics’ that enhance their combined effect in a positive direction.

Interestingly, the interaction between ‘quality’ and ‘semantics’ differs from the others. High quality scores interact more positively with ‘semantics’, and both features contribute positively to the model’s prediction, particularly when the quality score is around 0.6. Conversely, for values below than those thresholds, each attribute combination contributes negatively to the model’s prediction.

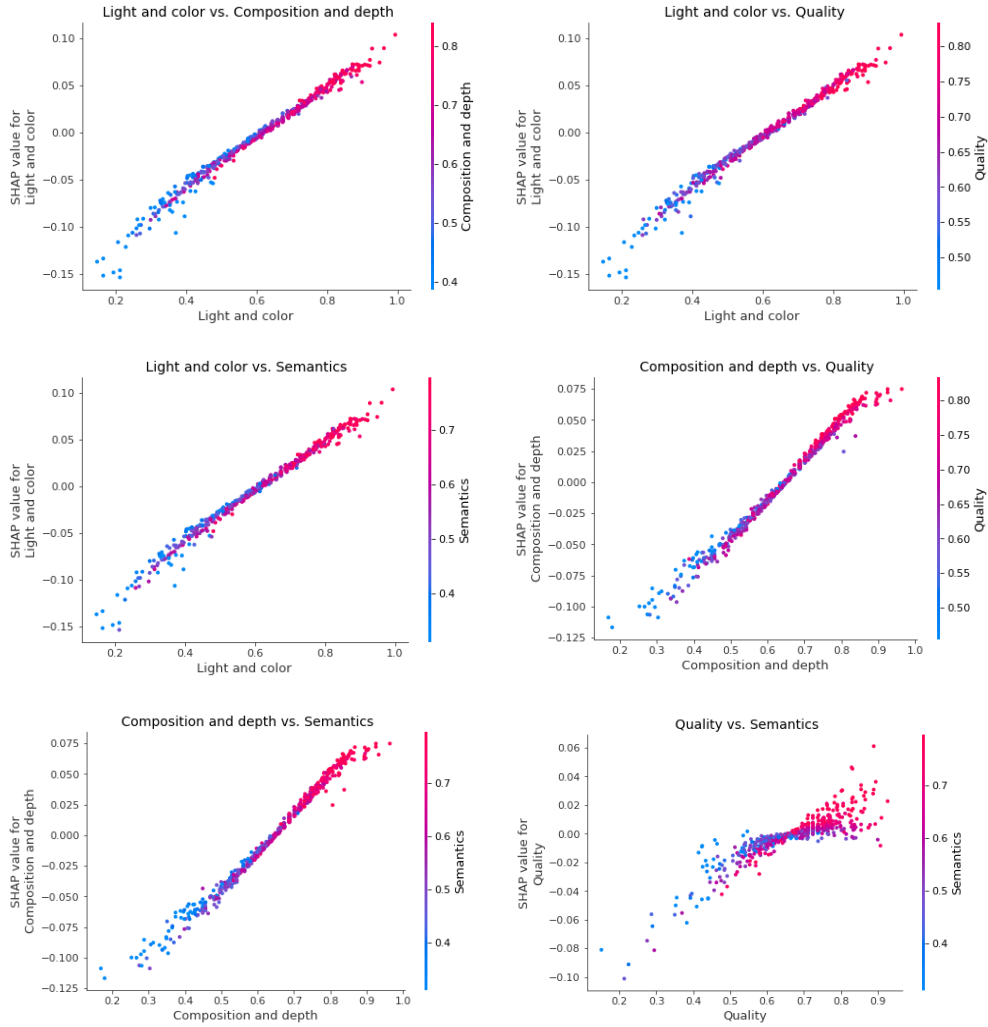


Fig. 8 Shap interaction plots for the EVA dataset based on SVR model.

5.3 Analysis Results on the PARA Dataset

The final dataset we use in our experiments is the PARA dataset [47]. As shown in Table 1, we utilize seven attribute scores as inputs for the machine learning models to predict the overall aesthetic scores of images. The results are presented in Table 4. Although all models exhibit similar performance, the SVR model once again demonstrates slightly better results. Hence, we apply the SHAP method to the SVR model to observe the importance of individual attributes in predicting overall aesthetic scores.

We present the SHAP summary plot for the PARA dataset in Figure 9. Here, the attribute ‘quality’ emerges as the most important feature in predicting the overall

Table 4 Performance of four machine learning models on the PARA dataset. We calculate all metrics on the test data to evaluate the generalization ability.

Model	R^2	MAE	MSE	RMSE	ρ
Random forest	0.9841	0.0550	0.0048	0.0696	0.988
Multilayer perceptron	0.9839	0.0555	0.0049	0.0701	0.989
XGBoost	0.9846	0.0542	0.0047	0.0685	0.989
Support vector regression	0.9854	0.0530	0.0044	0.0667	0.989

aesthetic scores. It is followed by ‘content’, ‘composition’, ‘color’, ‘light’, ‘depth of field’, and ‘object emphasis’, respectively. Interestingly, quality appears at the bottom of the SHAP summary plot for the EVA dataset in Figure 7, but it holds the top position in the SHAP summary plot for the PARA dataset. The other three machine learning models also yield the same result for ‘quality’ in their SHAP summary plots, as seen in the Appendix E. In the PARA dataset, ‘quality’ represents the overall judgement of image quality [47]. In the EVA dataset, the question for each attribute was phrased as ‘How do you like this attribute?’ [43]. The difference in the importance of ‘quality’ in the two datasets may be caused by the way the question was asked or the subjective nature of the attribute.

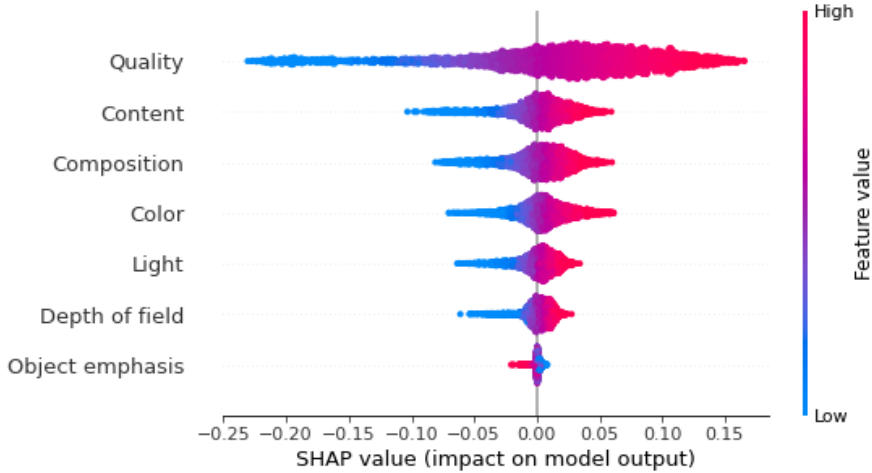


Fig. 9 Shap summary plot for the PARA dataset based on the SVR model.

In the PARA dataset, which includes a total of 7 attributes, several interesting interactions between these attributes come to light. Figure 10 showcases some notable examples of these interactions as observed in the SHAP values between aesthetic attributes. The rest of the interaction plots are available in the Appendix F. One notable observation is that low values of the combination of ‘quality’ and ‘object emphasis’ tend to increase the model’s output. This pattern holds consistent for each attribute combination with ‘object emphasis’. Apart from this, we observe positive

interactions between the other attributes. For example, when the quality score is higher than 0.4, it interacts with composition, reinforcing their combined effect in a positive direction. A similar pattern is observed for the attribute ‘light’ when paired with ‘content’. On the other hand, when the depth of field score falls below 0.6, both this attribute and light contribute negatively to the model’s prediction.

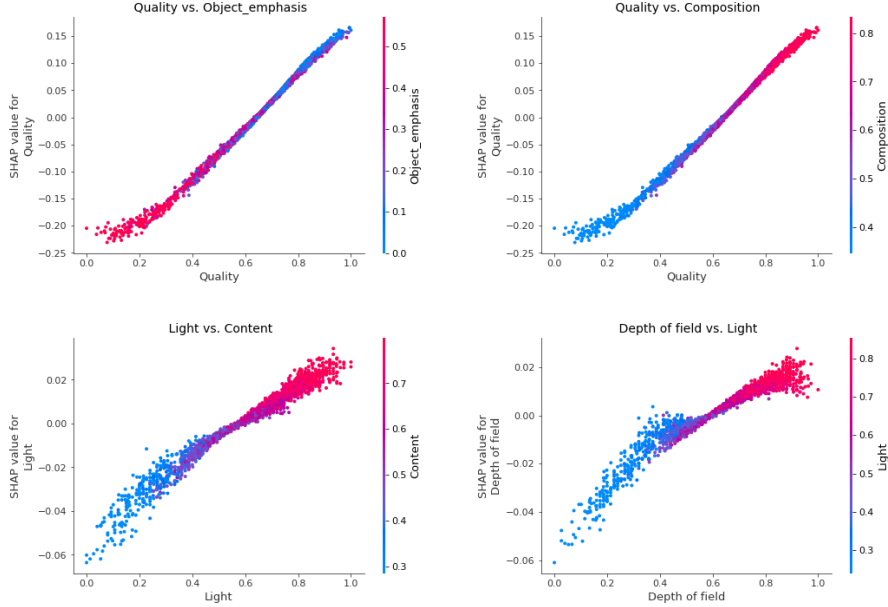


Fig. 10 Selected attribute interaction plots for the PARA dataset based on the SVR model.

6 Conclusion

In this study, we have undertaken a new perspective of image aesthetics preferences by focusing on attribute scores and utilizing various machine learning models to predict overall aesthetic scores. Our emphasis on explainable AI, particularly the SHAP method, has allowed us to gain valuable insights into the contributions of individual attributes to the model’s predictions. We observe the factors influencing image aesthetics and shed light on the interpretability and explainability of our machine learning models. Moreover, we apply the SHAP method in the field of computational aesthetics for the first time, also allowing us to examine the interactions between the features.

It is essential to acknowledge the inherent subjectivity of aesthetic preferences. Therefore, the quality and diversity of the dataset play a critical role in the performance and interpretability of our models. In this study, we utilize three image aesthetic assessment benchmarks, each with its own set of attributes and ratings per image. As a result, our data-dependent models may yield slightly different results. The importance of having a well-curated and diverse dataset cannot be understated, as it significantly impacts the generalization and robustness of our findings.

Furthermore, examining multiple machine learning models enhances the consistency of results. Through this novel approach for aesthetics research and the application of explainable AI techniques, we hope to enhance our understanding of aesthetics in images, contributing to the field of computational aesthetics. Ultimately, our efforts aim to enhance the overall understanding and appreciation of image aesthetics through computational methods.

Acknowledgments. Funded by the European Union (ERC AdG, GRAPPA, 101053925, awarded to Johan Wagemans). Views and opinions expressed are however those of the authors only and do not necessarily reflect those of the European Union or the European Research Council Executive Agency. Neither the European Union nor the granting authority can be held responsible for them.

Appendix A Attributes in the AADB dataset

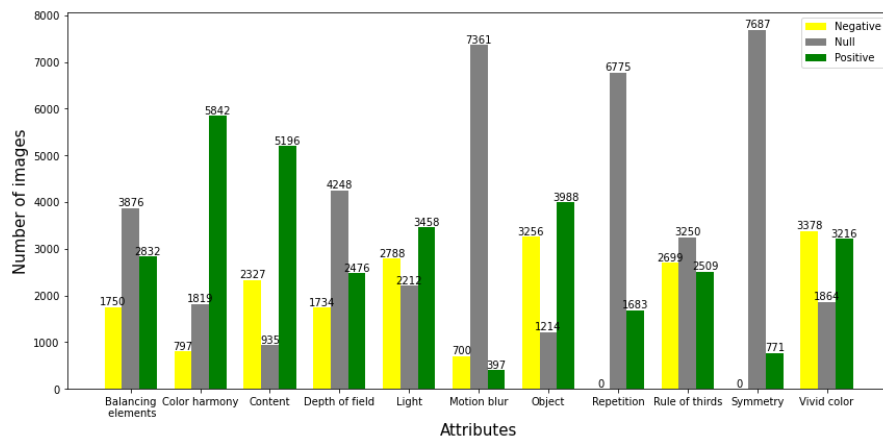


Fig. A1 Illustration of negative, null, and positive ratings for each attribute in the training set of AADB dataset [9, 42].

Appendix B SHAP summary plots for Random Forest, XGBoost, and MLP for the AADB dataset

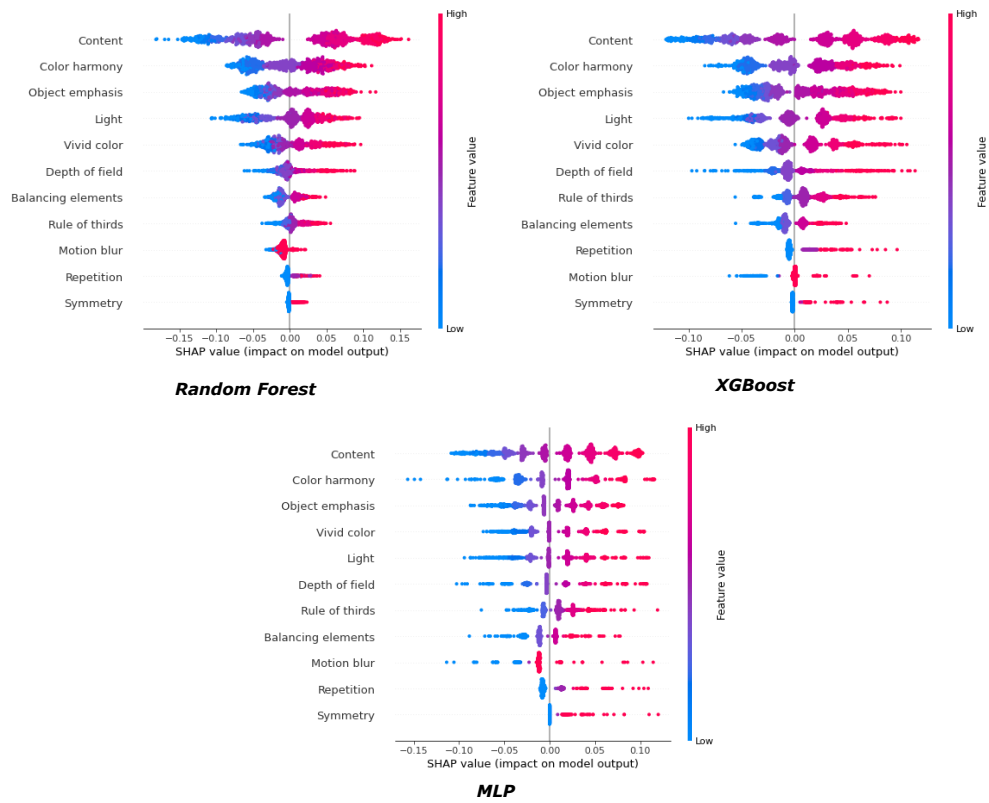


Fig. B2 Shap summary plots for the AADB dataset based on Random Forest, XGBoost and MLP models.

Appendix C Interaction plots for the AADB dataset

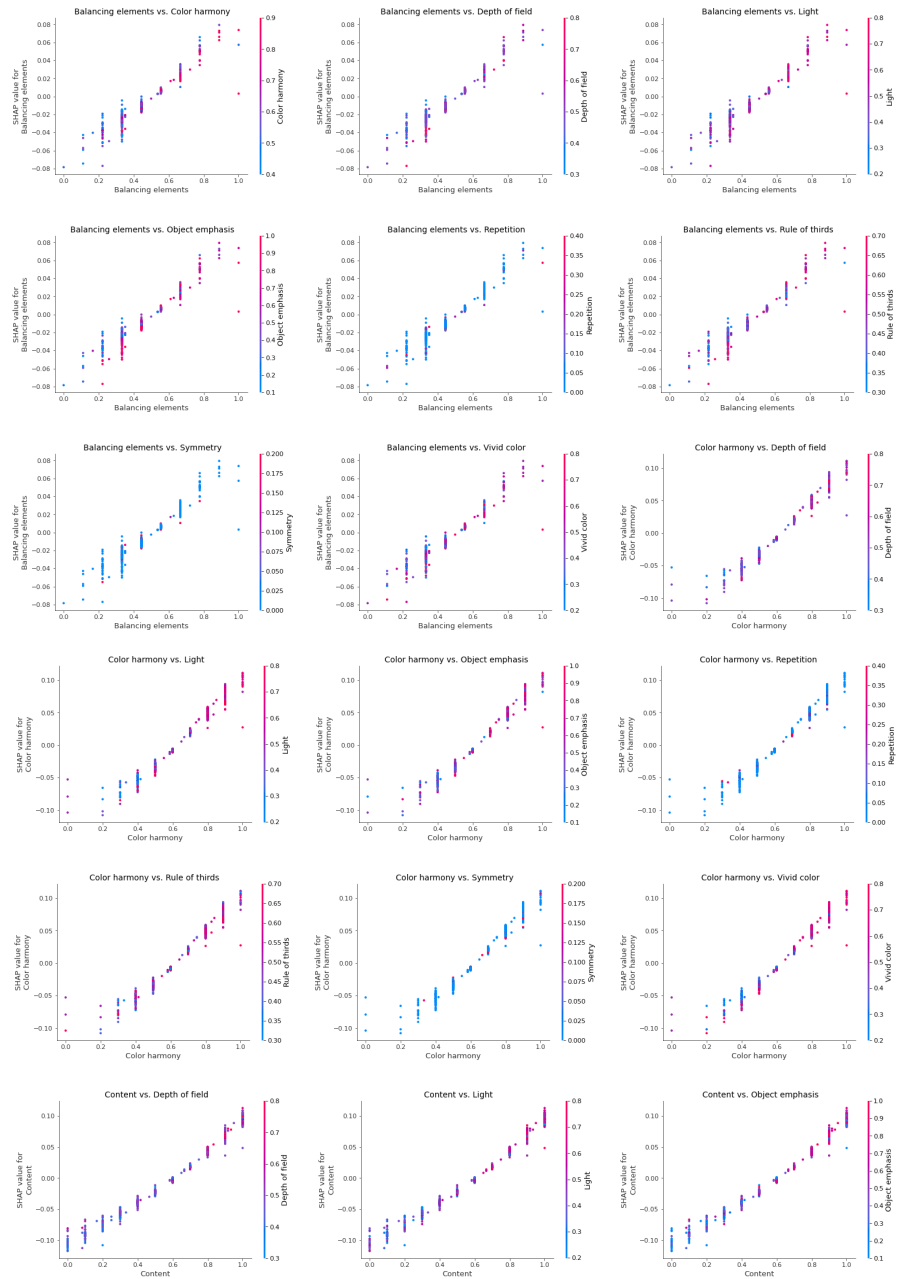


Fig. C3 Interaction plots for the AADB dataset based on the SVR model (part I).

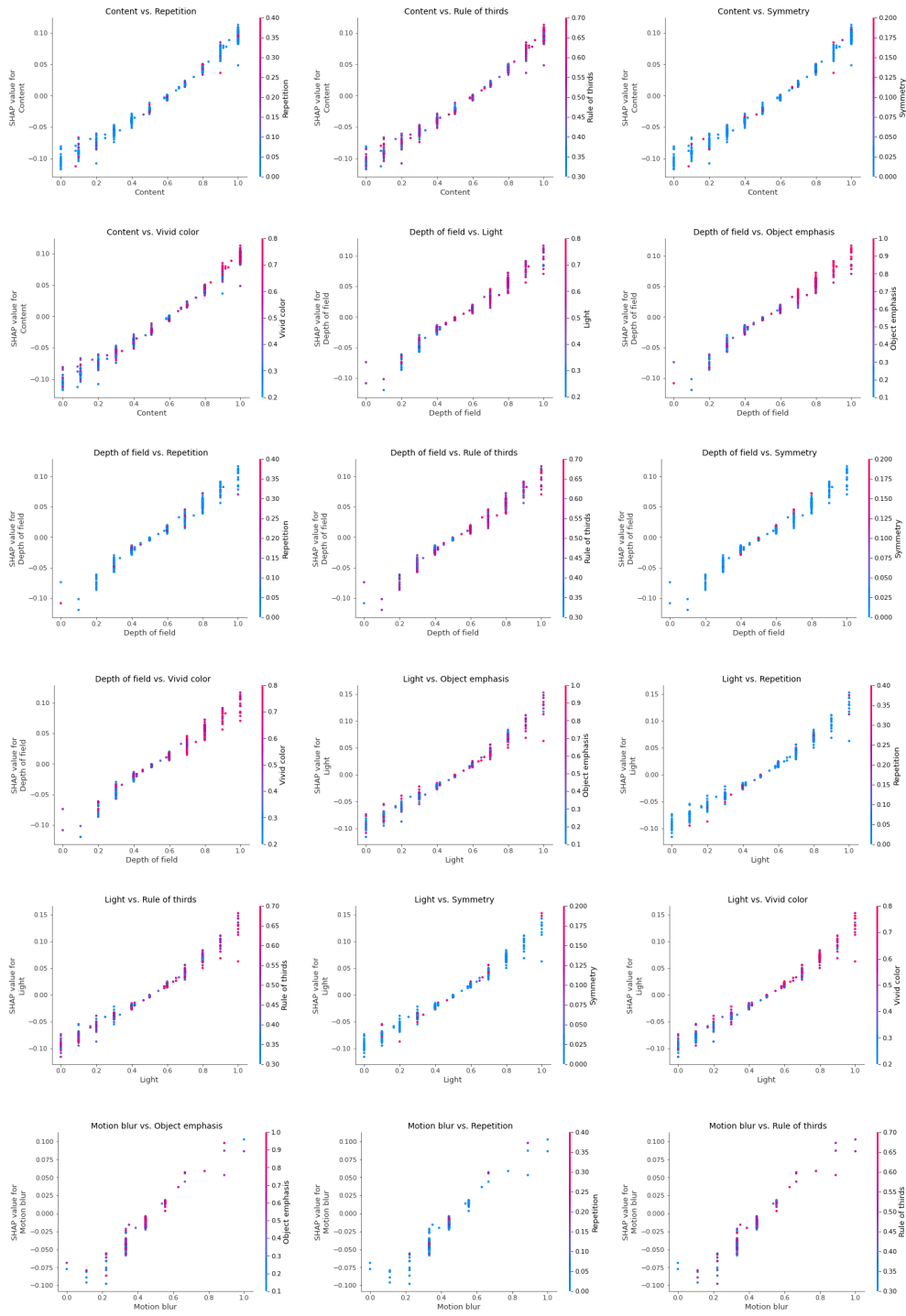


Fig. C4 Interaction plots for the AADB dataset based on the SVR model (part II).

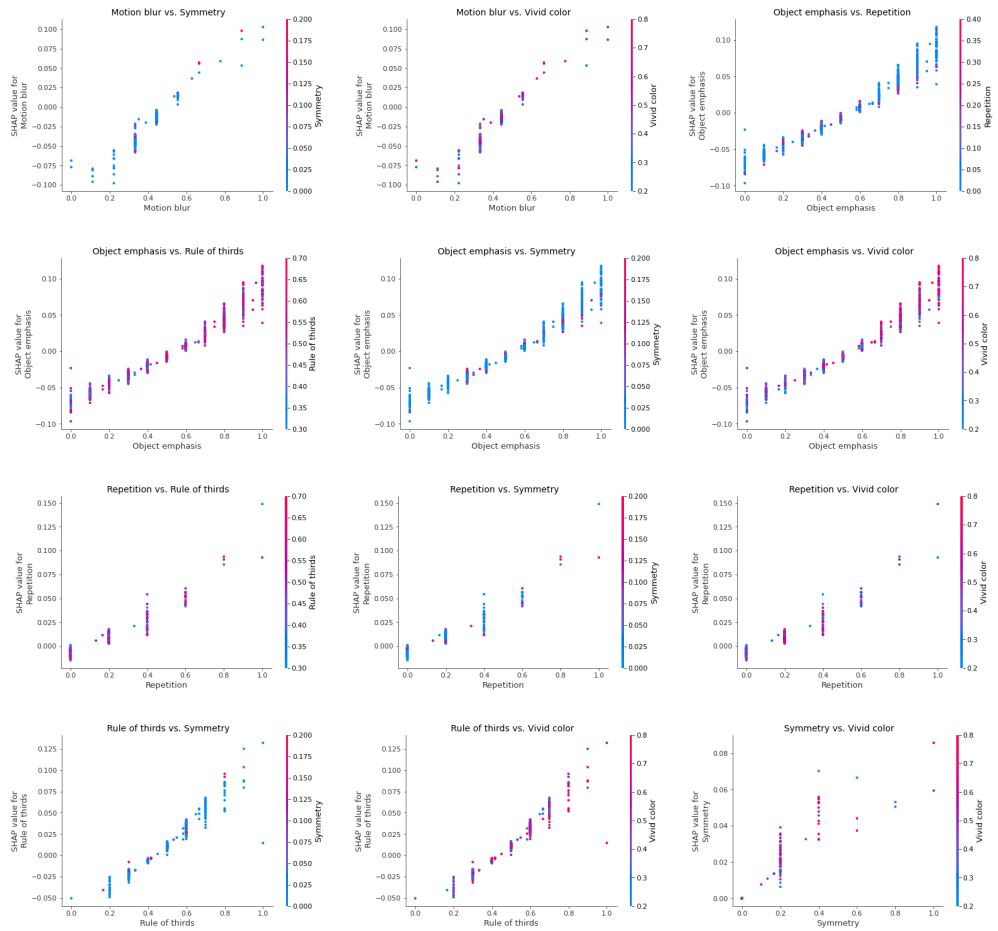


Fig. C5 Interaction plots for the AADB dataset based on the SVR model (part III).

Appendix D SHAP summary plots for Random Forest, XGBoost, and MLP for the EVA dataset

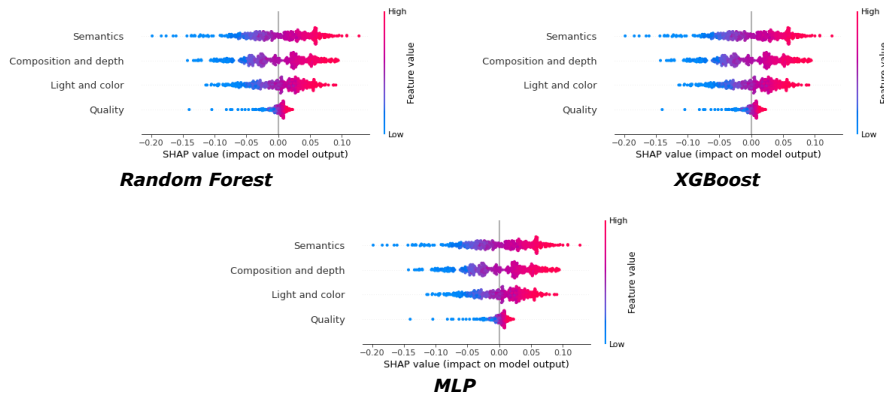


Fig. D6 Shap summary plots for the EVA dataset based on Random Forest, XGBoost and MLP models.

Appendix E SHAP summary plots for Random Forest, XGBoost, and MLP for the PARA dataset

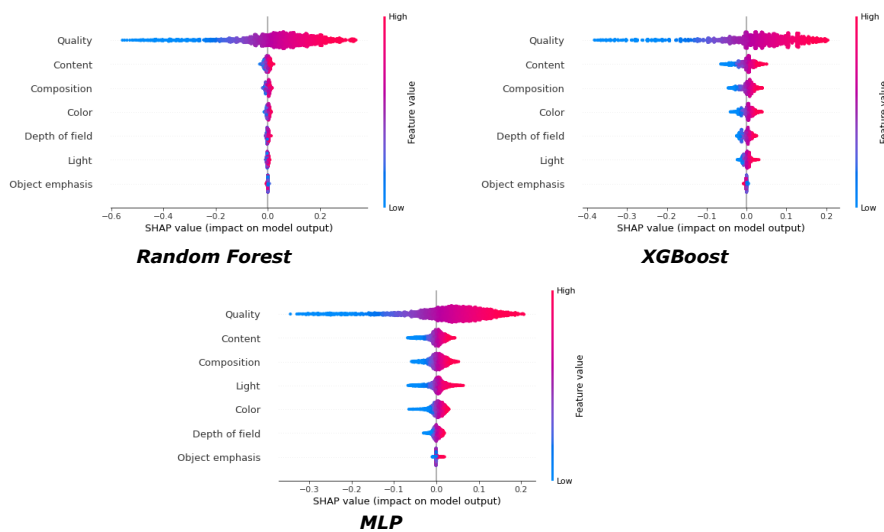


Fig. E7 Shap summary plots for the PARA dataset based on Random Forest, XGBoost and MLP models.

Appendix F Interaction plots for the PARA dataset

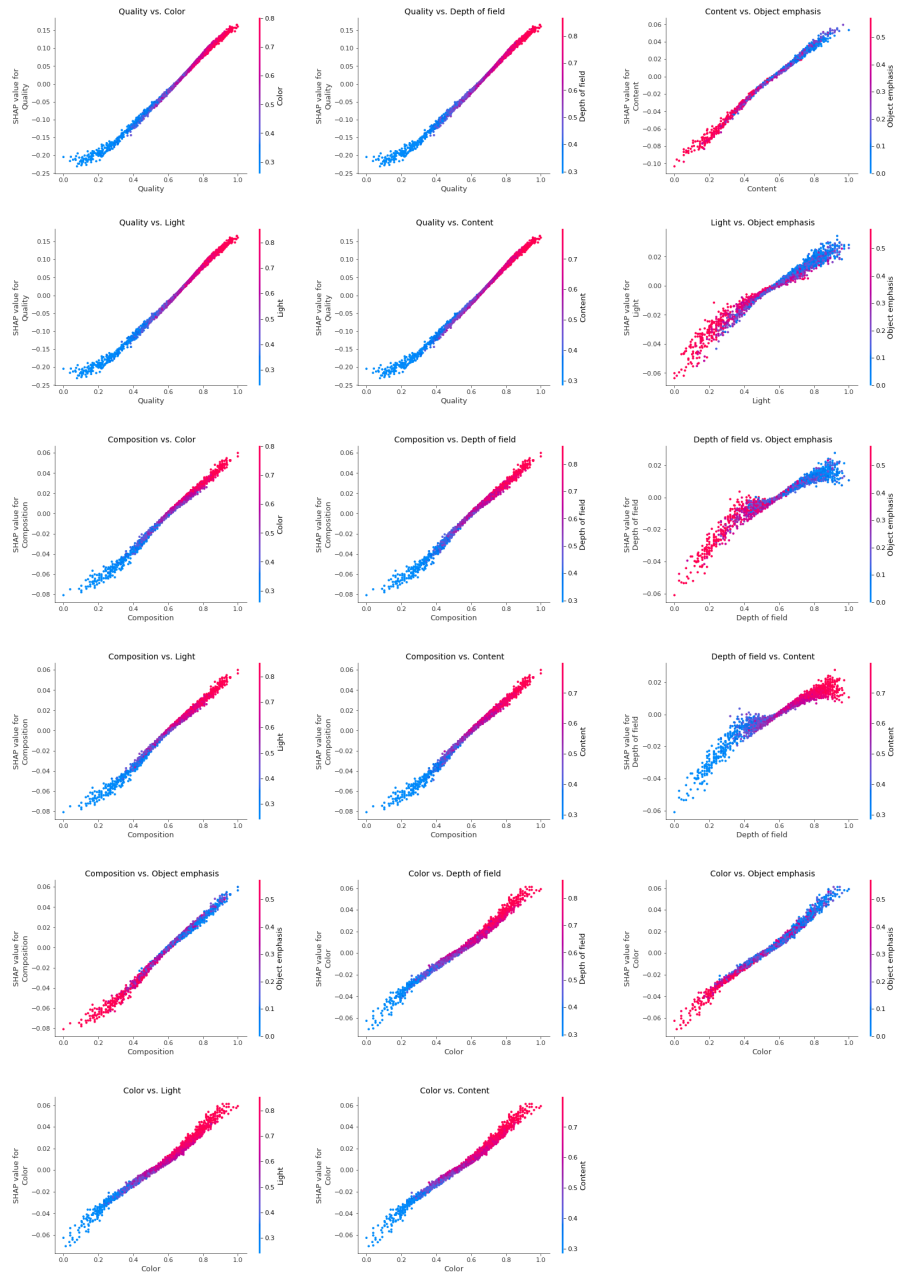


Fig. F8 Interaction plots for the PARA dataset based on the SVR model.

References

- [1] Nadal, M., Vartanian, O.: The oxford handbook of empirical aesthetics. Oxford University Press (2019)
- [2] Deng, Y., Loy, C.C., Tang, X.: Image aesthetic assessment: An experimental survey. *IEEE Signal Processing Magazine*, 80–106 (2017)
- [3] Hoenig, F.: Defining computational aesthetics. *Computational aesthetics in graphics, visualization and imaging*, 13–18 (2005)
- [4] Brachmann, A., Redies, C.: Computational and experimental approaches to visual aesthetics. *Frontiers in Computational Neuroscience* **11** (2017)
- [5] Valenzise, G., Kang, C., Dufaux, F.: Advances and challenges in computational image aesthetics. *Human perception of visual information: psychological and computational perspectives* (2022)
- [6] Lu, X., Lin, Z., Jin, H., Yang, J., Wang, J.Z.: RAPID: Rating pictorial aesthetics using deep learning. *Proceedings of the 22nd ACM International Conference on Multimedia*, 457–466 (2014)
- [7] Talebi, H., Milanfar, P.: NIMA: Neural image assessment. *IEEE Transactions on Image Processing* **27(8)**, 3998–4011 (2018)
- [8] Pan, B., Wang, S., Jiang, Q.: Image aesthetic assessment assisted by attributes through adversarial learning. *Proceedings of the AAAI Conference on Artificial Intelligence* **33**, 679–686 (2019)
- [9] Soydaner, D., Wagemans, J.: Multi-task convolutional neural network for image aesthetic assessment. *arXiv preprint arXiv: 2305.09373* (2023)
- [10] Celona, L., Leonardi, M., Napoletano, P., Rozza, A.: Composition and style attributes guided image aesthetic assessment. *IEEE Transactions on Image Processing* **31**, 5009–5024 (2022)
- [11] Li, L., Huang, Y., Wu, J., Yang, Y., Li, Y., Guo, Y., Shi, G.: Theme-aware visual attribute reasoning for image aesthetics assessment. *IEEE Transactions on Circuits and Systems for Video Technology* (2023)
- [12] Li, L., Zhu, T., Chen, P., Yang, Y., Li, Y., Lin, W.: Image aesthetic assessment with attribute-assisted multimodal memory network. *IEEE Transactions on Circuits and Systems for Video Technology* (2023)
- [13] Lundberg, S.M., Lee, S.I.: A unified approach to interpreting model predictions. *Advances in Neural Information Processing Systems* **30** (2017)

- [14] Drucker, H., Burges, C.J.C., Kaufman, L., Smola, A., Vapnik, V.: Support vector regression machines. *Advances in Neural Information Processing Systems* 9 (1996)
- [15] Boser, B.E., Guyon, I.M., Vapnik, V.N.: A training algorithm for optimal margin classifiers. *Proceedings of the Fifth Annual Workshop on Computational Learning Theory*, 144–152 (1992)
- [16] Ho, T.K.: Random decision forests. *Proceedings of Third International Conference on Document Analysis and Recognition* 1, 278–282 (1995)
- [17] Alpaydm, E.: *Introduction to machine learning*. The MIT Press (2014)
- [18] Géron, A.: *Hands-On Machine Learning with Scikit-Learn & Tensorflow*. O’Reilly Media, Inc., 1005 Gravenstein Highway North, Sebastopol, CA 95472 (2017)
- [19] Breiman, L.: Random forests. *Machine Learning* 45, 5–32 (2001)
- [20] Breiman, L.: Bagging predictors. *Machine Learning* 24, 123–140 (1996)
- [21] Chen, T., Guestrin, C.: XGBoost: A scalable tree boosting system. *Proceedings of the 22nd ACM SIGKDD International Conference on Knowledge Discovery and Data Mining*, 785–794 (2016)
- [22] Schapire, R.E.: The strenght of weak learnability. *Machine Learning* 5, 197–227 (2017)
- [23] Friedman, J.: Greedy function approximation: a gradient boosting machine. *Annals of Statistics* 29(5), 1189–1232 (2001)
- [24] Goodfellow, I., Bengio, Y., Courville, A.: *Deep learning*. MIT Press (2016)
- [25] Schölkopf, B., Smola, A.J.: *Learning with kernels: support vector machines, regularization, optimization, and beyond*. MIT Press (2002)
- [26] Rumelhart, D.E., Hinton, G.E., Williams, R.J.: Learning representations by back-propagating errors. *Nature*, 533–536 (1986)
- [27] Yuksel, E., Soydaner, D., Bahtiyar, H.: Nuclear binding energy predictions using neural networks: Application of the multilayer perceptron. *International Journal of Modern Physics E* 30(03), 2150017 (2021)
- [28] Ouyang, L., et al.: Training language models to follow instructions with human feedback. *Advances in Neural Information Processing Systems* 35, 27730–27744 (2022)
- [29] Krizhevsky, A., Sutskever, I., Hinton, G.: Imagenet classification with deep convolutional neural networks. *Advances in neural information processing systems*

25 (2012)

- [30] Ramesh, A., et al.: Zero-shot text-to-image generation. International conference on machine learning, 8821–8831 (2021)
- [31] Biran, O., Cotton, C.: Explanation and justification in machine learning: A survey. IJCAI-17 Workshop on Explainable AI (XAI) **8(1)**, 8–13 (2017)
- [32] Linardatos, P., Papastefanopoulos, V., Kotsiantis, S.: Explainable AI: A review of machine learning interpretability methods. Entropy **23** (2020)
- [33] Gohel, P., Singh, P., Mohanty, M.: Explainable AI: current status and future directions. arXiv preprint arXiv: 2107.07045 (2021)
- [34] Holzinger, A., Saranti, A., Molnar, C., Biecek, P., Samek, W.: Explainable AI methods - a brief overview. Lecture Notes in Computer Science **13200** (2022)
- [35] Ribeiro, M.T., Singh, S., Guestrin, C.: Why should i trust you?: explaining the predictions of any classifier. Proceedings of the 22nd ACM SIGKDD International Conference on Knowledge Discovery and Data Mining, 1135–1144 (2016)
- [36] Shrikumar, A., Greenside, P., Kundaje, A.: Learning important features through propagating activation differences. International Conference on Machine Learning **70**, 3145–3153 (2017)
- [37] Shapley, L.S.: A value for n-person games. Contributions to the Theory of Games, 307–317 (1953)
- [38] Winter, E.: The shapley value. Handbook of Game Theory with Economic Applications **3**, 2025–2054 (2002)
- [39] Molnar, C.: Interpretable machine learning: A guide for making black box models explainable. Independently published (2022)
- [40] Broeck, G.V., Lykov, A., Schleich, M., Suci, D.: On the tractability of SHAP explanations. Journal of Artificial Intelligence Research **74**, 851–886 (2022)
- [41] Lahiri, A., Alipour, K., Adeli, E., Salimi, B.: Combining counterfactuals with shapley values to explain image models. International Conference on Machine Learning (2022)
- [42] Kong, S., Shen, X., Lin, Z., Mech, R., Fowlkes, C.: Photo aesthetic ranking network with attributes and content adaptation. European Conference on Computer Vision, 662–679 (2016)
- [43] Kang, C., Valenzise, G., Dufaux, F.: EVA: An explainable visual aesthetics dataset. Joint Workshop on Aesthetic and Technical Quality Assessment of Multimedia and Media Analytics for Societal Trends, 5–13 (2020)

- [44] Shaham, U., Zaidman, I., Svirsky, J.: Deep ordinal regression using optimal transport loss and unimodal output probabilities. arXiv preprint arXiv:2011.07607 (2021)
- [45] Li, L., Zhi, T., Shi, G., Yang, Y., Xu, L., Li, Y., Guo, Y.: Anchor-based knowledge embedding for image aesthetics assessment. *Neurocomputing* (2023)
- [46] Duan, J., Chen, P., Li, L., Wu, J., Shi, G.: Semantic attribute guided image aesthetics assessment. *IEEE International Conference on Visual Communications and Image Processing (VCIP)*, 1–5 (2022)
- [47] Yang, Y., Xu, L., Li, L., Q., N., Li, Y., Zhang, P., Guo, Y.: Personalized image aesthetics assessment with rich attributes. *Proceedings of the IEEE/CVF Conference on Computer Vision and Pattern Recognition*, 19861–19869 (2022)
- [48] Fang, Y., Zhu, H., Zeng, Y., Ma, K., Wang, Z.: Perceptual quality assessment of smartphone photography. *Proceedings of the IEEE/CVF Conference on Computer Vision and Pattern Recognition*, 3677–3686 (2020)
- [49] Hosu, V., Lin, H., Sziranyi, T., Saupe, D.: KonIQ-10k: An ecologically valid database for deep learning of blind image quality assessment. *IEEE Transactions on Image Processing* **29**, 4041–4056 (2020)
- [50] Glorot, X., Bordes, A., Bengio, Y.: Deep sparse rectifier neural networks. *Proceedings of the Fourteenth International Conference on Artificial Intelligence and Statistics*, 315–323 (2011)
- [51] Glorot, X., Bengio, Y.: Understanding the difficulty of training deep feedforward neural networks. *Proceedings of the Thirteenth International Conference on Artificial Intelligence and Statistics*, 249–256 (2010)
- [52] Kingma, D., Ba, J.: A method for stochastic optimization. arXiv preprint arXiv:1412.6980 (2014)
- [53] Soydaner, D.: A comparison of optimization algorithms for deep learning. *International Journal of Pattern Recognition and Artificial Intelligence* **34(13)**, 2052013 (2020)